




Engineered *bacillus subtilis* enhances bone regeneration via immunoregulation and anti-Infection

Fang-Sheng Fu^{a,1}, Huan-Huan Chen^{b,c,1}, Yu Chen^a, Ying Yuan^a, Yong Zhao^a, Aixi Yu^{a,**}, Xian-Zheng Zhang^{a,b,*} 

^a Department of Orthopedic Trauma and Microsurgery, Zhongnan Hospital of Wuhan University, Wuhan, 430071, PR China

^b Key Laboratory of Biomedical Polymers of Ministry of Education & Department of Chemistry, Wuhan University, Wuhan, 430072, PR China

^c State Key Laboratory of Biocatalysis and Enzyme Engineering, Hubei Key Laboratory of Industrial Biotechnology, School of Life Sciences, Hubei University, Wuhan, 430062, PR China

ARTICLE INFO

Keywords:

Chronic osteomyelitis
Bacillus subtilis
Antibacterial
Engineered probiotic hydrogel
Immunoregulation

ABSTRACT

Chronic osteomyelitis caused by implant infections is a common complication following orthopedic surgery. Preventing bacterial infection and simultaneously improving bone regeneration are the key for osteomyelitis. Current treatments include systemic antibiotics and multiple surgical interventions, but the strategies available for treatment are limited. In this study, a multifunctional engineered *Bacillus subtilis* (*B. sub*) hydrogel with sulfasalazine (SSZ) is developed to treat methicillin-resistant *Staphylococcus aureus* (MRSA) infection and anti-inflammatory and promote bone regeneration. *B. sub* in alginate hydrogels protects *B. sub* from being cleared by the host immune system while allowing the release of its bioactive substances, including antibacterial peptides and anti-inflammatory agents such as SSZ. The results show that the engineered probiotic hydrogels exhibit excellent antibacterial efficacy against MRSA (97 %) and prevent the development of bacterial resistance. The antibacterial effect is primarily mediated through the secretion of bioactive peptides by *B. sub*, which not only inhibit MRSA growth but also reduce the likelihood of resistance development. Meanwhile, the probiotic hydrogel has a greater ability to induce M2 polarization of macrophages and promote angiogenesis, resulting in enhanced osteogenic differentiation in bone marrow mesenchymal stem cells (BMSCs) and thus enhancing bone regeneration. This engineered probiotic hydrogel offers a promising strategy by simultaneously combating bacterial infection and enhancing osteogenic differentiation for chronic osteomyelitis.

1. Introduction

Infections associated with implants, which enhance bacterial colonization and inhibit bone formation, are significant contributors to the persistence of chronic osteomyelitis [1]. Surgeries involving fractures and joint replacements frequently necessitate the use of implants, thereby elevating the risk of osteomyelitis. The primary manifestations include infection, bone destruction, recurrence, and chronic inflammation [2–4]. Although various microorganisms can cause osteomyelitis, approximately 75 % of cases are caused by Staphylococci. Methicillin-resistant *Staphylococcus aureus* (MRSA) is particularly concerning due to its high resistance to many commonly used antibiotics

and its ability to form biofilms on implant surfaces [5]. The primary approach to treating implant-associated infections involves the use of systemic or local antibiotics [5–7]. However, systemic antibiotics often have limited penetration into bone tissue, and local antibiotics, such as those delivered via antibiotic-loaded bone cement, lose efficacy once the active agents are depleted, potentially leaving behind a nidus for reinfection. Debridement and drainage surgeries are commonly performed to remove infected tissue or implants, but they are invasive and may compromise bone integrity, often requiring multiple procedures. Despite these efforts, chronic osteomyelitis is particularly challenging to treat due to the formation of bacterial biofilms, the emergence of antibiotic-resistant strains, and the need for simultaneous bone

* Corresponding author. Department of Orthopedic Trauma and Microsurgery, Zhongnan Hospital of Wuhan University, Wuhan 430071, PR China.

** Corresponding author.

E-mail addresses: fufangshengs@163.com (F.-S. Fu), chenhh1008@whu.edu.cn (H.-H. Chen), a1114780674@outlook.com (Y. Chen), 2011302180067@whu.edu.cn (Y. Yuan), mocuishle@163.com (Y. Zhao), yuaixi@whu.edu.cn (A. Yu), xz-zhang@whu.edu.cn (X.-Z. Zhang).

¹ These authors contributed equally to this work.

regeneration. The overuse of antibiotics in recent years has led to the global issue of bacterial resistance [8,9]. When implant-associated infections progress to antibiotic-resistant bacterial infections, the resulting antibiotic resistance can lead to surgical failure, amputation, or even death [10,11].

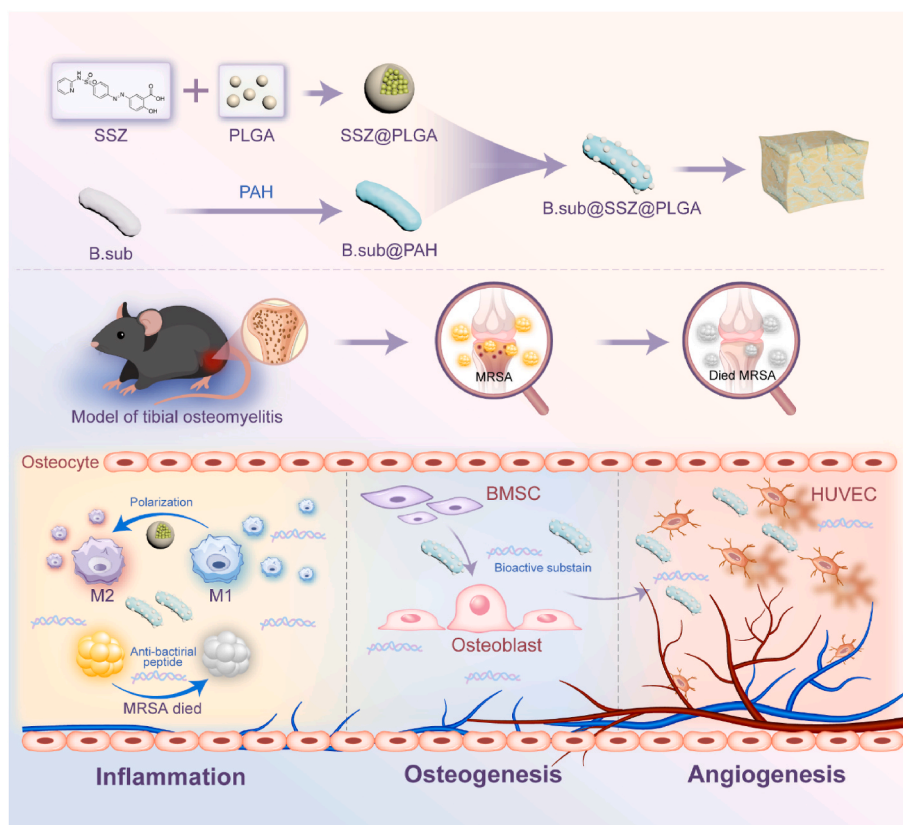
Current clinical treatments for implant-associated infections include debridement, fenestration and drainage, antibiotic irrigation, and implantation of antibiotic bone cement [12,13], remain limited in their ability to address both infection control and bone regeneration. During the antibiotic treatment process, once the effective antimicrobial components are exhausted, their ability to combat the infection diminishes. There is an urgent need for a durable alternative therapy specifically targeting MRSA-induced osteomyelitis.

Microbe-mediated therapies has attracted significant attention [14–17]. Combination therapies using live probiotics and anti-inflammatory drugs have shown promise for treating osteomyelitis, particularly due to their ability to simultaneously address both infection and inflammation. For osteomyelitis therapy, some probiotics such as *Lactobacillus plantarum*, *Lactobacillus casei* exhibit anti-infection ability [18–20]. As non-pathogenic bacteria, probiotics have the functions of inhibiting the pathogenic bacterium and regulating the body microenvironment [21]. Numerous studies have been conducted to combine probiotics with nanomaterials through physical and chemical interactions, to design functionally active materials with multiple effects for anti-bacterial infection or tissue regeneration [21–25]. *Bacillus subtilis* (*B.sub*), a Food and Drug Administration (FDA)-approved probiotic, has been widely used for bacterial and fungal infections due to its unique antibacterial effects [26–29]. Several studies have reported that *B.sub* disrupts the quorum-sensing regulatory system by producing fengycins [27], inhibits *Staphylococcus aureus* adhesion and biofilm formation by producing surfactins [30], and enhances the antimicrobial function of macrophages [31]. However, an ideal treatment strategy for

osteomyelitis should have multifunctional biofunctions to prevent bacterial infection and promote bone regeneration.

Sulfasalazine (SSZ) was recognized for its potent anti-inflammatory and immunosuppressive effects, particularly in the treatment of inflammatory bowel disease and rheumatoid arthritis [32,33]. A recent study reported that pharmacological inhibition or gene knockout targeting SLC7A11 promotes the bactericidal function of macrophages, reduces bacterial load in the bone, and improves bone structure in mice with *Staphylococcus aureus* osteomyelitis [34]. Moreover, SSZ, as an inhibitor of SLC7A11, has also been used in the treatment of osteomyelitis. Therefore, the study explores the use of therapeutic nanodrug-modified probiotics to synergistically enhance the therapeutic effects of probiotics.

Considering the above functions of probiotic, we hypothesized that a live bacterial formulation, capable of consistently producing antimicrobial molecules at the infection site, could serve as an alternative therapy of osteomyelitis. To protect the probiotic from the host immune system, we designed a hydrogel encapsulation method that protects *B.sub* from host clearance, prevents its excessive proliferation, and ensures the consistent release of its active substances. Hydrogels are known to provide a conducive environment for nutrient transfer, cell growth and sensing, establishing them as highly favored materials for encapsulating living cells [35]. Additionally, SSZ is modified on the surface of *B.sub* to improve the inflammatory bone microenvironment. *B.sub* is modified with poly (allylamine hydrochloride) (PAH) to acquire a positive charge, while the poly (lactic-co-glycolic) acid (PLGA)-coated nanoparticles containing SSZ (SSZ@PLGA) carry a negative charge. *B.sub* is combined with SSZ@PLGA through electrostatic interactions, yielding a biohybrid *B.sub*@SSZ@PLGA (Scheme 1). To evade attacks from the host's immune system, *B.sub* are encapsulated within a hydrogel matrix using the gelation properties of sodium alginate in the presence of calcium ions. This bioactive biohybrid exhibits multiple



Scheme 1. Illustration showing the preparation and osteomyelitis treatment of the engineered probiotic hydrogel. The probiotic hydrogel could antibacterial, pro-osteogenesis, and pro-angiogenesis through antibacterial peptide and bioactive substance secreted by *B.sub*.

functions. Firstly, antimicrobial peptides continuously secreted by living *B. sub* effectively inhibits the growth of *Staphylococcus aureus*. Secondly, this bioactive material can be injected into the bone marrow cavity for minimally invasive treatment. Simultaneously, SSZ reduces the immunogenicity of *B. sub* and modulates the inflammatory response by converting pro-inflammatory M1 macrophages into anti-inflammatory M2 macrophages through the regulation of SLC7A11, thereby enhancing the immune-regulatory activity of the local bone microenvironment and accelerating tissue repair. Lastly, these bioactive substances promote osteoblast mineralization and microvascular formation, facilitating bone tissue regeneration. These combined effects effectively control the progression of osteomyelitis, accelerate bone tissue regeneration, and better fill bone marrow cavities, thereby achieving more effective treatment.

2. Results and discussion

2.1. Preparation and characterization of *B.sub*@SSZ@PLGA biohybrids and hydrogel beads

The preparation experiment of *B. sub*@SSZ@PLGA biohybrids is illustrated in Fig. 1a. PLGA nanoparticles loaded with SSZ (SSZ@PLGA) were prepared using the single emulsion method and then combined with positively charged *B. sub* modified with PAH to synthesize *B. sub*@SSZ@PLGA biohybrids. The synthesized SSZ@PLGA nanoparticles exhibited a uniform size distribution with an average diameter of 207.57 nm (Fig. 1b, Fig. S1) and a zeta potential of -15.4 mV (Fig. 1c). *B. sub* modified with PAH had a positively charged with a zeta potential of 23.9 mV (Fig. 1c). The negatively charged SSZ@PLGA nanoparticles and positively charged *B. sub* were held together through electrostatic interactions. As shown in Fig. 1d, scanning electron microscopy (SEM) and transmission electron microscopy (TEM) images clearly revealed significant aggregation of SSZ@PLGA nanoparticles on the surface of *B. sub*. To assess the effect of *B. sub*@SSZ@PLGA on

bacterial proliferation, we compared the colony counts on Luria-Bertani (LB) agar plates after 24 h of incubation. There was no significant difference in colony counts between the pure *B. sub* and the *B. sub*@SSZ@PLGA biohybrids (Fig. 1e and f), indicating that the integration of PAH and SSZ@PLGA nanoparticles did not affect the viability of *B. sub*.

We encapsulated live *B. sub* in alginate to create 1 mm diameter hydrogel beads and stored at 4 °C, which protected the probiotic from immune system attack without hindering the release of bioactive substances and facilitates the quantification of live probiotics [22,36]. SEM analysis of the hydrogel beads, as shown in Fig. S2, revealed that the pore size of the hydrogel is smaller than the diameter of *B. sub*, suggesting that the probiotics are effectively retained within the hydrogel and unlikely to leak out. Release result revealed the sustained release behavior of SSZ from SSZ@PLGA and *B. sub*@SSZ@PLGA hydrogel beads, with approximately 50 % (SSZ@PLGA) and 60 % (*B.sub*@SSZ@PLGA) release ratios within 240 h (Fig. 1g). In the *B. sub*@SSZ@PLGA group, the release rate of SSZ was faster, likely due to the ability of *B. sub* to promote the degradation of PLGA, which accelerated the release of SSZ. In a similar bacterial viability experiment, we crushed and diluted the hydrogel beads after 20 days at 4 °C and found that the probiotics were still remain viable (Fig. S3a). To investigate the fate of pure *B. sub* and *B. sub*@SSZ@PLGA hydrogel in vivo, it was implanted subcutaneously in mice. As shown in Figs. S3b and S3c, no bacterial colonies were detectable in the pure *B. sub* group after 5 days, whereas *B. sub*@SSZ@PLGA hydrogel group remained detectable even after 20 days. This indicates that without the protective effect of the hydrogel, the probiotics were rapidly cleared by the host. To evaluate the local retention time of *B. sub*@SSZ@PLGA hydrogels in vivo, CY5.5-NHS-labeled engineered probiotics were either encapsulated with or without hydrogel and then locally injected into the tibial bone marrow cavity of mice. The retention time was assessed using IVIS imaging. As shown in Fig. S4, the fluorescence signal from unencapsulated probiotics disappeared within 5 days, whereas *B. sub*@SSZ@PLGA

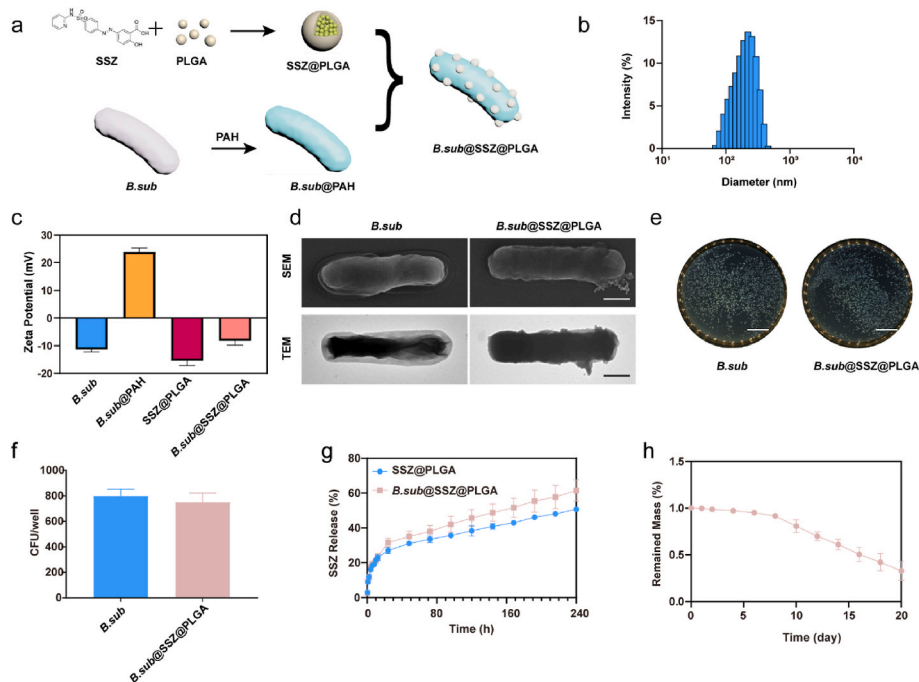


Fig. 1. Characterization and property of *B. sub*@SSZ@PLGA. (a) Schematic illustration of the synthesis of *B. sub*@SSZ@PLGA. (b) The hydrated diameter of the SSZ@PLGA nanoparticles. (c) Zeta potential changes during the preparation of *B. sub*@SSZ@PLGA. (d) SEM and TEM image of *B. sub* and *B. sub*@SSZ@PLGA biohybrids. The scale bar is 500 nm. (e) Images of the bacterial colonies of *B. sub* and *B. sub*@SSZ@PLGA. The scale bar is 2 cm. (f) Quantitative analysis of bacterial colonies for *B. sub* and *B. sub*@SSZ@PLGA. (g) The release curve of SSZ from SSZ@PLGA and *B. sub*@SSZ@PLGA hydrogel beads. (h) In vitro degradation of *B. sub*@SSZ@PLGA hydrogel beads under PBS condition and 37 °C.

hydrogel persisted for nearly 24 days. These results demonstrate that the hydrogel provides protection for probiotics against clearance by the host, enabling prolonged local activity and sustained therapeutic effects. In vitro degradation results of *B. sub*@SSZ@PLGA hydrogel showed a gradual weight loss over the experimental period, indicating its

controlled degradation profile. The hydrogel retained 80 % of its original mass after 10 days and 30 % after 20 days (Fig. 1h). These results indicated that the activity of *B. sub* was not affected by PAH and the combination with SSZ@PLGA, demonstrating the successful preparation of *B. sub*@SSZ@PLGA hydrogel. The integration of *B. sub* with

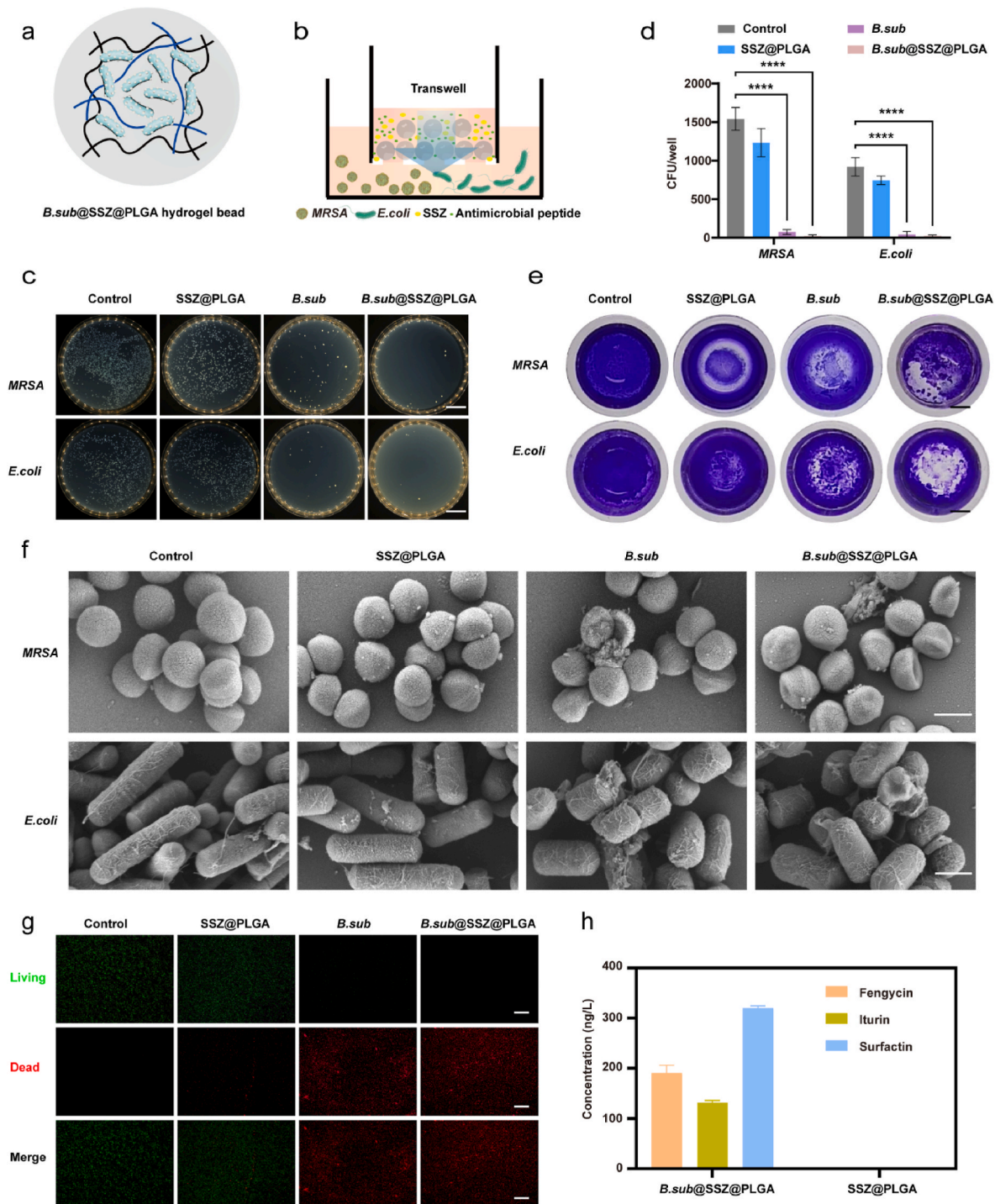


Fig. 2. Antibacterial performance of *B. sub*@SSZ@PLGA hydrogel beads in vitro. (a) Schematic of *B. sub*@SSZ@PLGA hydrogel bead. (b) Illustration of *B. sub*@SSZ@PLGA hydrogel beads antibacterial at transwell. (c) Agar plate photos of MRSA and *E. coli* under different treatments (Control (treated with saline), SSZ@PLGA, *B. sub* and *B. sub*@SSZ@PLGA). Images are representative of at least three independent experiments. The scale bar is 2 cm. (d) CFU counts for MRSA and *E. coli* after the abovementioned treatment. (e) Biofilm images of MRSA and *E. coli* under different treatments; the bacterium were stained with crystal violet. The scale bar is 4 mm. (f) Representative SEM images of MRSA and *E. coli* before and after different treatment. Images are representative of at least three independent experiments. The scale bar is 1 μ m. (g) Live/Dead Staining of MRSA staining with SYTO 9 (green) and Propidium iodide (PI, red) after different treatment for 24 h. Images are representative of at least three independent experiments. The scale bar is 30 μ m. (h) The expression of fengycin, surfactin, and iturin was detected by ELISA kit in the supernatants of SSZ@PLGA and *B. sub*@SSZ@PLGA hydrogel beads. Data are presented as mean \pm SD (n = 3) (**** $P < 0.0001$).

SSZ@PLGA into the hydrogel not only retained the functionality of the probiotics but also demonstrated potential for delivering bioactive agents effectively, laying the foundation for its therapeutic applications.

2.2. Antibacterial performance of *B. sub*@SSZ@PLGA hydrogel beads *in vitro*

B. sub, an aerobic gram-positive bacteria, is a probiotic commonly found in the environment [37]. It has been reported to secrete antimicrobial peptides and exert a quorum-sensing effect within the gut microbiota [27,38]. We hypothesized that the antimicrobial peptides secreted by *B. sub* could disrupt cell membrane structures, leading to bacterial apoptosis and preventing the development of antibiotic resistance. In this study, we evaluated the antibacterial efficacy of *B. sub*@SSZ@PLGA hydrogel beads against MRSA and *Escherichia coli* (*E. coli*). The antibacterial effect was determined by counting colony-forming units (CFUs). As shown in Fig. 2b, hydrogel beads were co-cultured with MRSA or *E. coli* for 24 h, plated on LB agar plates, and the resulting colonies were counted. We found that the number of colonies significantly decreased in the groups treated with *B. sub* and *B. sub*@SSZ@PLGA hydrogel beads, indicating that nearly all MRSA (99 %) and *E. coli* (99 %) were killed (Fig. 2c and d). The *B. sub*@SSZ@PLGA group showed even more pronounced bactericidal effects. To verify the effect of *B. sub*@SSZ@PLGA hydrogel beads on biofilms, MRSA was suspended and cultured for 72 h to form biofilms. And then co-cultured with SSZ@PLGA, *B. sub*, or *B. sub*@SSZ@PLGA hydrogel beads for 24 h, followed stained by crystal violet. The results showed that *B. sub* and *B. sub*@SSZ@PLGA hydrogel beads were significantly more effective than the SSZ@PLGA group, demonstrating that living bacterial hydrogel beads could disrupt MRSA biofilm formation (Fig. 2e). We conducted similar experiments with *E. coli*, and obtained comparable results (Fig. 2c, d, e), indicating that live probiotic hydrogel beads were effective against both Gram-positive and Gram-negative bacteria. Using SEM, we observed the cellular morphology of MRSA and *E. coli* treated with *B. sub* and *B. sub*@SSZ@PLGA hydrogel beads. As depicted in Fig. 2f, MRSA and *E. coli* treated with *B. sub* and *B. sub*@SSZ@PLGA hydrogel beads exhibited abnormal morphologies, such as ruptured cell walls, cell shrinkage, and membrane contraction, while untreated bacterium showed normal shapes and intact cell membranes. Meanwhile, live/dead cell viability assays were conducted to evaluate the bactericidal effect of *B. sub*@SSZ@PLGA hydrogel against *E. coli* and MRSA. A higher proportion of bacterium exhibited red fluorescence in *B. sub* and *B. sub*@SSZ@PLGA hydrogel group compared to the untreated group (Fig. 2g and Fig. S5), indicating *B. sub* enhanced killing efficiency against these typical pathogens.

To investigate the bactericidal mechanism of *B. sub*@SSZ@PLGA hydrogel, we examined its production of antimicrobial peptides. Given that different *B. sub* subtypes produce distinct antimicrobial peptides, ELISA kits were used to detect three commonly produced peptides: surfactin, fengycin, and iturin. Supernatants from the *B. sub*@SSZ@PLGA hydrogel were collected at various time points. As shown in Fig. 2h, all three antimicrobial peptides were detected in the hydrogel supernatants, indicating that *B. sub* exerts its antibacterial effects through the secretion of these peptides.

These results suggest that the *B. sub*@SSZ@PLGA hydrogel exerts its antibacterial effects through the sustained release of antimicrobial peptides, including surfactin, fengycin, and iturin. These peptides demonstrate potent activity not only against Gram-positive bacterium like MRSA but also against Gram-negative bacterium like *E. coli*. The antimicrobial peptides may disrupt bacterial integrity by altering osmotic pressure across cell membranes or interacting with the cell walls. Furthermore, they are capable of breaking down mature biofilms, which are often resistant to conventional treatments. This broad-spectrum antimicrobial action highlights the versatility of this biohybrid system, making it a promising candidate for combating a wide range of bacterial infections, including those commonly associated with chronic

osteomyelitis.

2.3. *B. sub*@SSZ@PLGA hydrogel beads enhanced anti-inflammatory effects *in vitro*

Macrophage polarization can be divided into pro-inflammatory (M1) and anti-inflammatory (M2) types [39]. During the treatment of osteomyelitis, M2-type macrophages help establish the bone immune microenvironment and promote bone remodeling [40,41]. However, live bacterium can induce macrophage polarization towards M1-type macrophages [42], thereby accelerating the progression of osteomyelitis. To address this issue, we modified SSZ onto *B. sub* to leverage its anti-inflammatory properties and its role as an SLC7A11 inhibitor, aiming to promote the conversion of M1-type macrophages to M2-type macrophages [43]. After preparing the *B. sub*@SSZ@PLGA hydrogel beads, we assessed their effect on SLC7A11 expression in Raw264.7 cells using qPCR. The results showed that *B. sub*@SSZ@PLGA hydrogel beads significantly suppressed SLC7A11 expression (Fig. S6), confirming that the SSZ modified on *B. sub* effectively maintained its functional activity. Immunostaining and quantification revealed that, compared to the LPS group, the *B. sub*@SSZ@PLGA group exhibited a decrease in M1 macrophages and a significant increase in M2 macrophages (Fig. 3a and b). This result indicates that SSZ can effectively convert LPS-induced M1 macrophages into M2 macrophages. In contrast, unmodified *B. sub* hydrogel beads did not improve LPS-induced M1 polarization, while SSZ-modified live probiotic hydrogel beads significantly promoted the polarization of M1 macrophages to M2 macrophages. Flow cytometry analysis revealed that *B. sub*@SSZ@PLGA hydrogel beads increased the proportion of CD206⁺ (M2 phenotype) cells while decreasing the proportion of CD86⁺ (M1 phenotype) cells (Fig. 3c, d, e), indicating a shift towards an anti-inflammatory macrophage phenotype. On this basis, we further demonstrated that *B. sub*@SSZ@PLGA hydrogel beads effectively reduced the levels of pro-inflammatory cytokines such as TNF- α (Fig. 3f) while increasing the level of the anti-inflammatory cytokine IL-10 (Fig. 3g) by ELISA assay, indicating the anti-inflammatory properties of *B. sub*@SSZ@PLGA hydrogel beads.

These findings highlight the dual benefits of *B. sub*@SSZ@PLGA hydrogel beads in suppressing pro-inflammatory responses and enhancing anti-inflammatory effects, which are crucial for reducing inflammation and promoting tissue healing in osteomyelitis. The suppression of SLC7A11 likely facilitates the M1-to-M2 macrophage transition, supporting immune homeostasis.

2.4. *B. sub*@SSZ@PLGA hydrogel beads promoted the biomineralization of bone marrow mesenchymal stem cells *in vitro*

To investigate the effects of *B. sub*@SSZ@PLGA hydrogel beads on bone mineralization, it is essential to examine their impact on the proliferation and differentiation of bone marrow mesenchymal stem cells (BMSCs) into osteoblasts and mineralized nodules. Transwell assays were used to detect the effect of engineered probiotic hydrogel beads on BMSCs proliferation. Calcein staining results revealed that, compared to the control group, the *B. sub* group and *B. sub*@SSZ@PLGA group exhibited significantly higher BMSCs cell densities, indicating that live engineered probiotic hydrogel beads markedly promoted BMSCs proliferation (Fig. 4a and b). This effect is likely attributed to the bioactive substances released from the live probiotic hydrogel beads, which create a conducive microenvironment for BMSC growth. Differentiation of BMSCs into osteoblasts was assessed through alkaline phosphatase (ALP) staining, a marker of early osteogenic differentiation [44]. After 7 days of co-culture with live probiotic hydrogel beads, both the *B. sub* group and *B. sub*@SSZ@PLGA group showed greater ALP-positive areas compared to the control group (Fig. 4c). Quantitative analysis further confirmed significantly increased ALP activity, indicating enhanced osteogenic differentiation (Fig. 4d). To evaluate osteogenic mineralization, Alizarin Red S (ARS) staining was performed after 21 days of

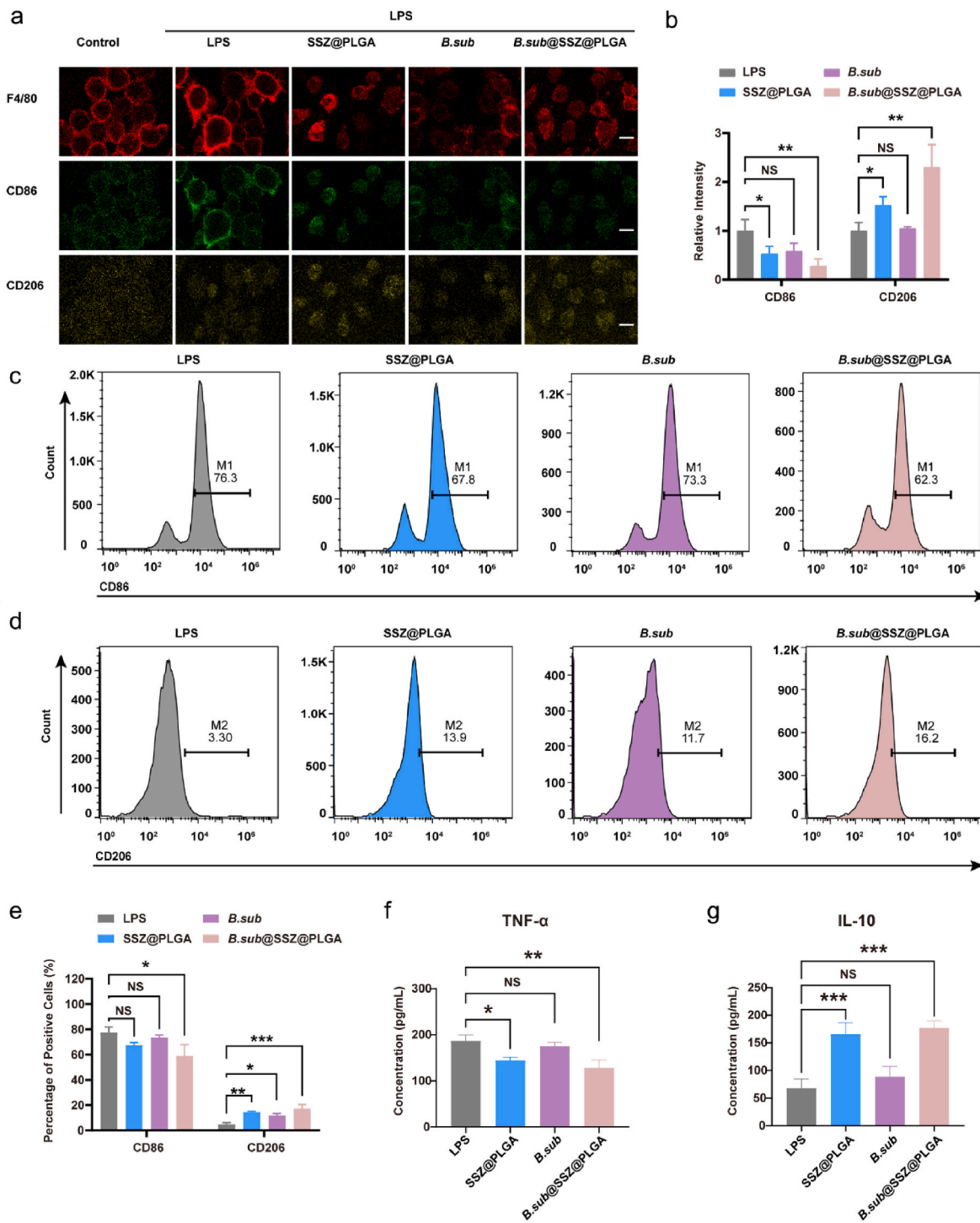


Fig. 3. Immunomodulation assay of *B. sub*@SSZ@PLGA hydrogel beads in vitro. (a–b) Representative images and quantification of the percentage of CD86⁺ and CD206⁺ cells in the LPS, SSZ@PLGA, *B. sub* and *B. sub*@SSZ@PLGA groups. The scale bar is 20 μm. (c–d) Flow cytometry histogram of (c) CD86⁺ and (d) CD206⁺ for RAW264.7 cultured in different conditions after stimulation of LPS. (e) Quantification of the percentage of CD86⁺ (M1 phenotype) and CD206⁺ (M2 phenotype) cells after polarization. (f–g) ELISA assays were performed to measure the levels of TNF-α (M1) and IL-10 (M2) in the supernatants from different treatment groups. Data are presented as mean ± SD (n = 3). (*P < 0.05, **P < 0.01, ***P < 0.001, NS: no significance).

co-culture. More ARS-positive areas were observed in the *B. sub* group and *B. sub*@SSZ@PLGA group (Fig. 4e and f). These results showed that live probiotic hydrogel beads enhanced osteogenic mineralization in vitro, with the *B. sub*@SSZ@PLGA group showing superior effects. To determine whether these effects are also evident at the genetic level, we examined the expression of osteoblast-specific genes, including ALP, runt-related transcription factor 2 (RUNX2), late osteogenesis gene

osteocalcin (OCN), collagen 1 (COL-1). By day 7, the expression of early osteogenic genes (ALP, RUNX2) was significantly upregulated in the *B. sub* and *B. sub*@SSZ@PLGA groups compared to the control group (Fig. 4g and h). By day 14, the expression of late osteogenic genes (OCN and COL-1) was also significantly enhanced (Fig. 4i and j). These results indicate that *B. sub*@SSZ@PLGA hydrogel beads effectively promote osteogenic differentiation and mineralization at the genetic level.

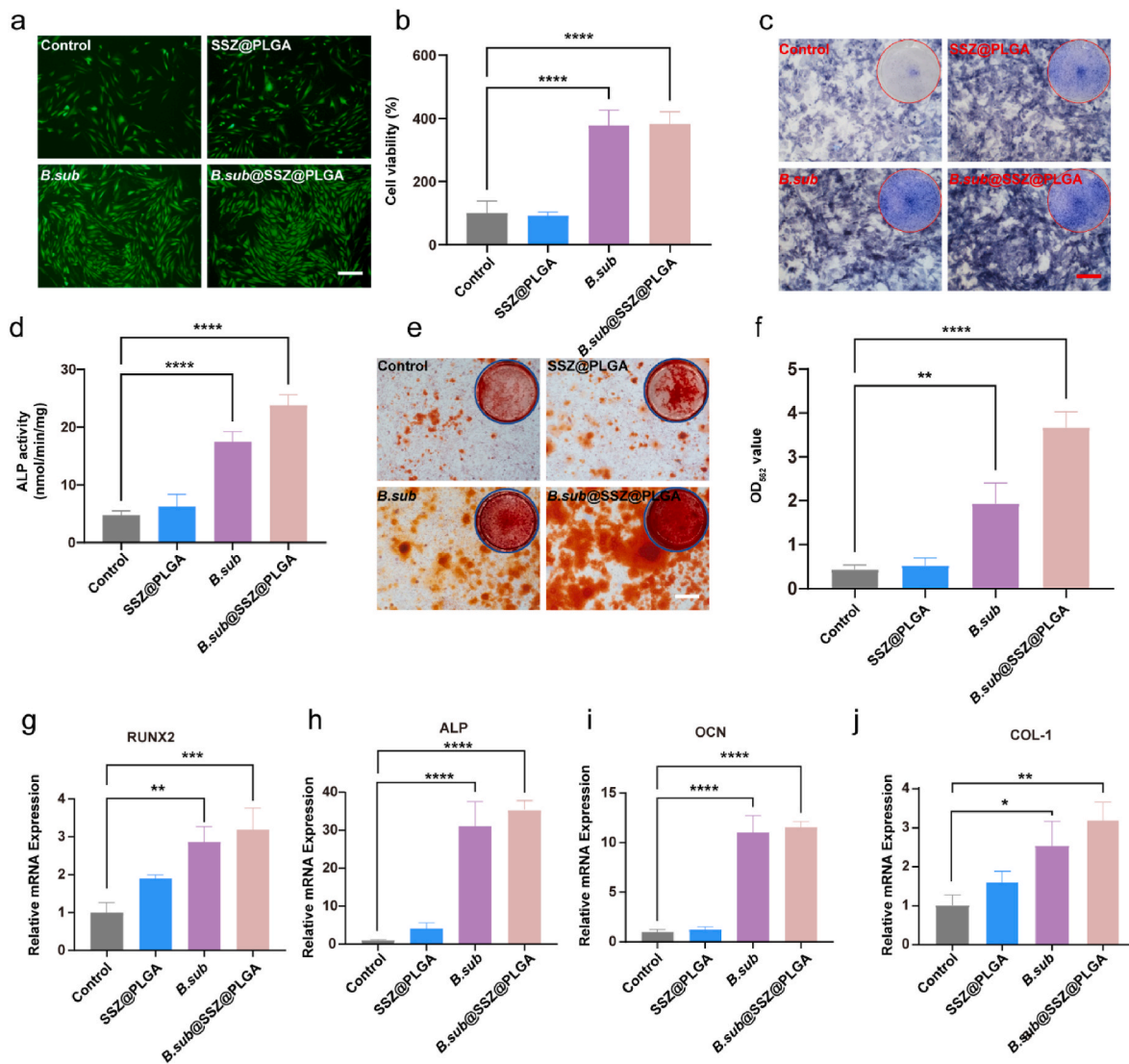


Fig. 4. Osteoblastic differentiation of BMSCs cultured with *B. sub*@SSZ@PLGA hydrogel beads in vitro. (a) Images of BMSCs under different treatments for 24 h. The scale bar is 200 μ m. The BMSCs were stained by Calcein-AM. (b) Quantitative analysis of HUVECs under different treatments for 24 h. (c) BMSCs were stained by ALP staining after co-cultured with different treatments for 7 days. The scale bar is 100 μ m. (d) ALP activity of BMSCs co-cultured with different treatments for 7 days. (e) Image ARS of BMSCs co-cultured with different treatments for 21 days. (f) Quantitative analysis of cell mineralization for 21 days. The scale bar is 100 μ m. (g–j) Osteogenic marker gene (RUNX2, OCN, ALP, COL-1) expression of BMSCs cultured with different treatment. Data are presented as mean \pm SD ($n = 3$) (** $P < 0.01$, *** $P < 0.001$, **** $P < 0.0001$).

In summary, *B. sub*@SSZ@PLGA hydrogel beads demonstrate a multi-faceted capability to promote bone regeneration. They not only support the proliferation of BMSCs but also significantly enhance osteogenic differentiation and mineralization. The upregulation of both early (ALP, RUNX2) and late (OCN, COL-1) osteogenic markers highlights their potential to regulate key stages of bone formation. These effects likely stem from the synergistic interaction between the live probiotics and the controlled release of SSZ, creating a bioactive environment conducive to osteogenesis.

2.5. *B. sub*@SSZ@PLGA hydrogel beads enhanced angiogenesis in vitro

Vascularization is crucial for bone regeneration, as an adequate blood supply provides the necessary nutrients, growth factors, and oxygen for regenerating bone tissue [45]. Previous experiments had demonstrated that *B. sub*@SSZ@PLGA hydrogel beads promoted osteoblast differentiation and facilitated bone formation. However, does *B. sub*@SSZ@PLGA also promote angiogenesis? This study investigates the effects of live probiotic hydrogel beads on the proliferation,

invasion, migration, and microvascular differentiation of human umbilical vein endothelial cells (HUVECs) to explore the impact of live probiotic hydrogel beads on angiogenesis. Firstly, we evaluated the effect of live probiotic hydrogel beads on HUVECs proliferation (Fig. 5a). After treating HUVECs with live probiotic hydrogel beads for 24 and 48 h, the CCK8 assay detected significant promotion of HUVECs proliferation in both *B. sub* and *B. sub*@SSZ@PLGA groups (Fig. 5b). To further examine the effect of live probiotic hydrogel beads on HUVECs invasion, HUVECs were cultured in the upper chamber of transwell and stained with crystal violet to observe the number and morphology of HUVECs under an inverted microscope. As shown in Fig. 5c, there were significant differences in the migration of HUVECs treated with *B. sub*@SSZ@PLGA hydrogel beads compared to other groups. Quantitative analysis (Fig. 5d) revealed a substantial increase in the number of invading cells in the *B. sub* and *B. sub*@SSZ@PLGA groups compared to the control group, indicating that live probiotic hydrogel beads markedly enhanced the invasion capability of HUVECs. To further assess the effect of live probiotic hydrogel beads on the migration ability of HUVECs, a scratch assay was performed on HUVECs cultured in the

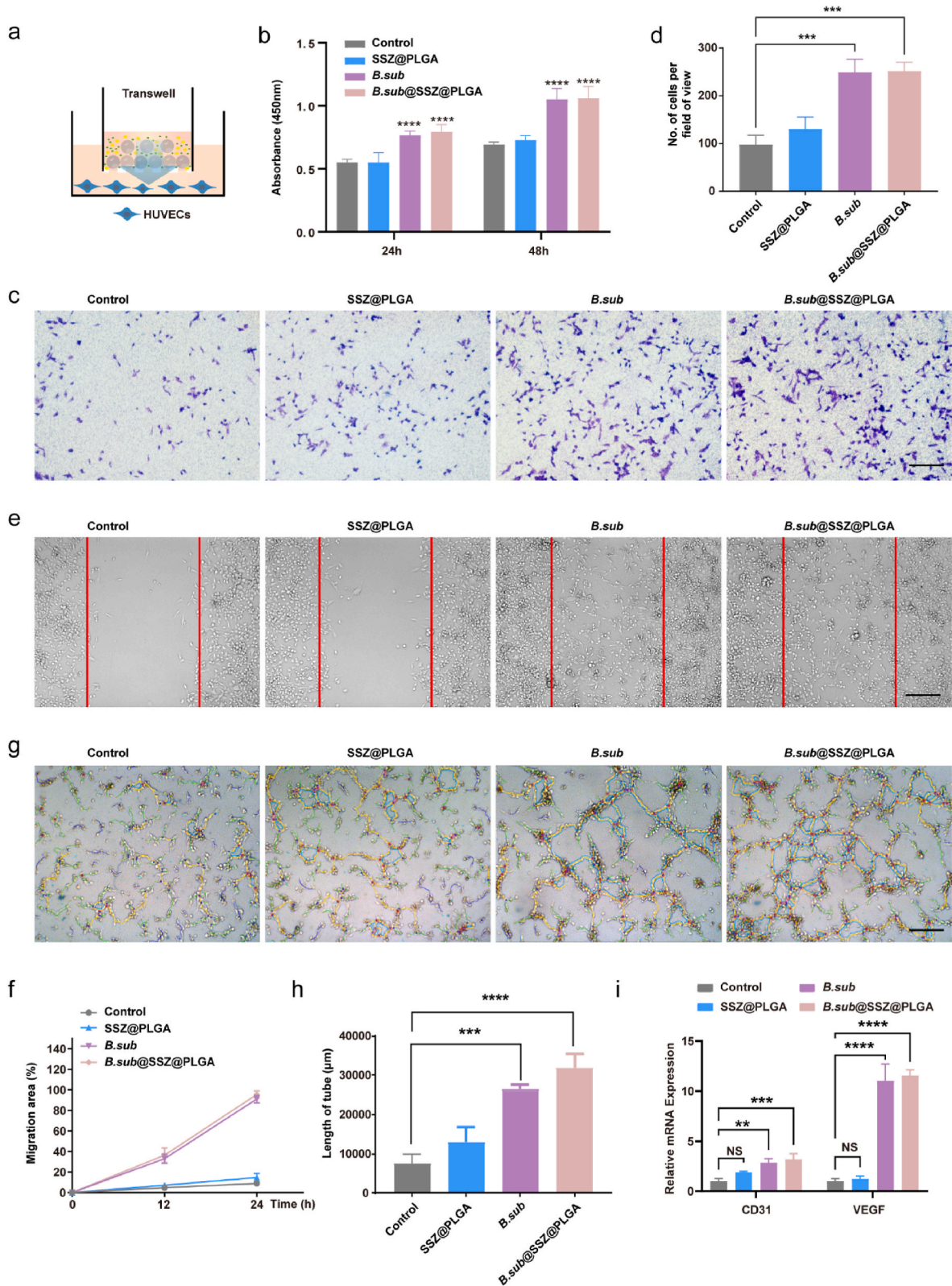


Fig. 5. Angiogenesis properties of *B. sub*@SSZ@PLGA hydrogel beads in vitro. (a) Illustration of *B. sub*@SSZ@PLGA hydrogel beads pro-angiogenesis at transwell. (b) HUVECs viability detected by CCK8 under different treatments for 24 h and 48 h. (c–d) Representative images and number of invasive HUVECs by in the transwell assay; the HUVECs were stained with crystal violet. The scale bar is 100 μm. (e–f) Representative images and quantification of HUVECs’ migration at 24 h. The scale bar is 100 μm. (g–h) Representative images and quantification of the HUVECs’ tube formation about length of tube. The scale bar is 200 μm; the HUVECs were colored by Imagej. (i) Angiogenesis-related genes (CD31 and VEGF) expression of HUVECs cultured with different treatment. Data are presented as mean ± SD (n = 3) (***p* < 0.001, ****p* < 0.001, *****p* < 0.0001, NS: no significance).

lower chamber of the transwell. The horizontal migration capacity of HUVECs was measured at 0 h and 12 h (Fig. S7). As shown in Fig. 5e, the cell-free area significantly decreased after 24 h in HUVECs treated with live probiotic hydrogel beads compared to the control group. Quantitative analysis of the migration area showed a similar trend, with the migration area of HUVECs in the *B. sub* and *B. sub*@SSZ@PLGA groups reaching approximately 92 % and 95 %, respectively (Fig. 5f). This indicated that the active substances secreted by *B. sub* not only promoted HUVECs proliferation but also accelerated HUVECs invasion and migration. Additionally, to evaluate the effect of *B. sub*@SSZ@PLGA hydrogel beads on angiogenesis, a Matrigel tube formation assay was performed. The changes of tube structure, branch points, tube meshes and tube length was observed under an inverted microscope after 24 h. As expected, the tube formation in the *B. sub* and *B. sub*@SSZ@PLGA groups was significantly increased (Fig. 5g and h, Figure S8). The bioactive substances secreted by *B. sub* could promote HUVECs endothelial cell proliferation, invasion, migration, and angiogenesis. On a molecular level, the expression of angiogenesis-specific genes, including CD31 and VEGF (vascular endothelial growth factor), was evaluated. By day 3, we observed a significant upregulation of these angiogenesis-related genes in the *B. sub* and *B. sub*@SSZ@PLGA groups, compared to the control group (Fig. 5i).

In summary, *B. sub*@SSZ@PLGA hydrogel beads demonstrated significant pro-angiogenic effects, underscoring their potential in bone regeneration by enhancing vascularization. The hydrogel beads markedly promoted HUVECs proliferation, invasion, and migration, with quantitative assays revealing substantial increases in cell activity and tube formation. These effects were further validated by the upregulation of angiogenesis-related genes CD31 and VEGF at the molecular level. These findings suggest that the synergistic action of live probiotics and bioactive SSZ supports the creation of a vascularized microenvironment, highlighting their translational potential in bone tissue engineering and regenerative medicine.

2.6. Antibacterial properties and pro-osteogenesis of *B. sub*@SSZ@PLGA hydrogel in vivo

Implant infections are a common postoperative complication that significantly increases the risk of bacterial colonization after implantation [46–48]. To establish an implant infection model, MRSA were introduced into the tibial medullary cavity of C57BL/6J mice, followed by the implantation of a steel implant (Fig. 6a, Fig. S9). One week after the establishment of the animal model, chronic osteomyelitis was confirmed by Micro-CT (Fig. S10b) followed by plate culture and colony

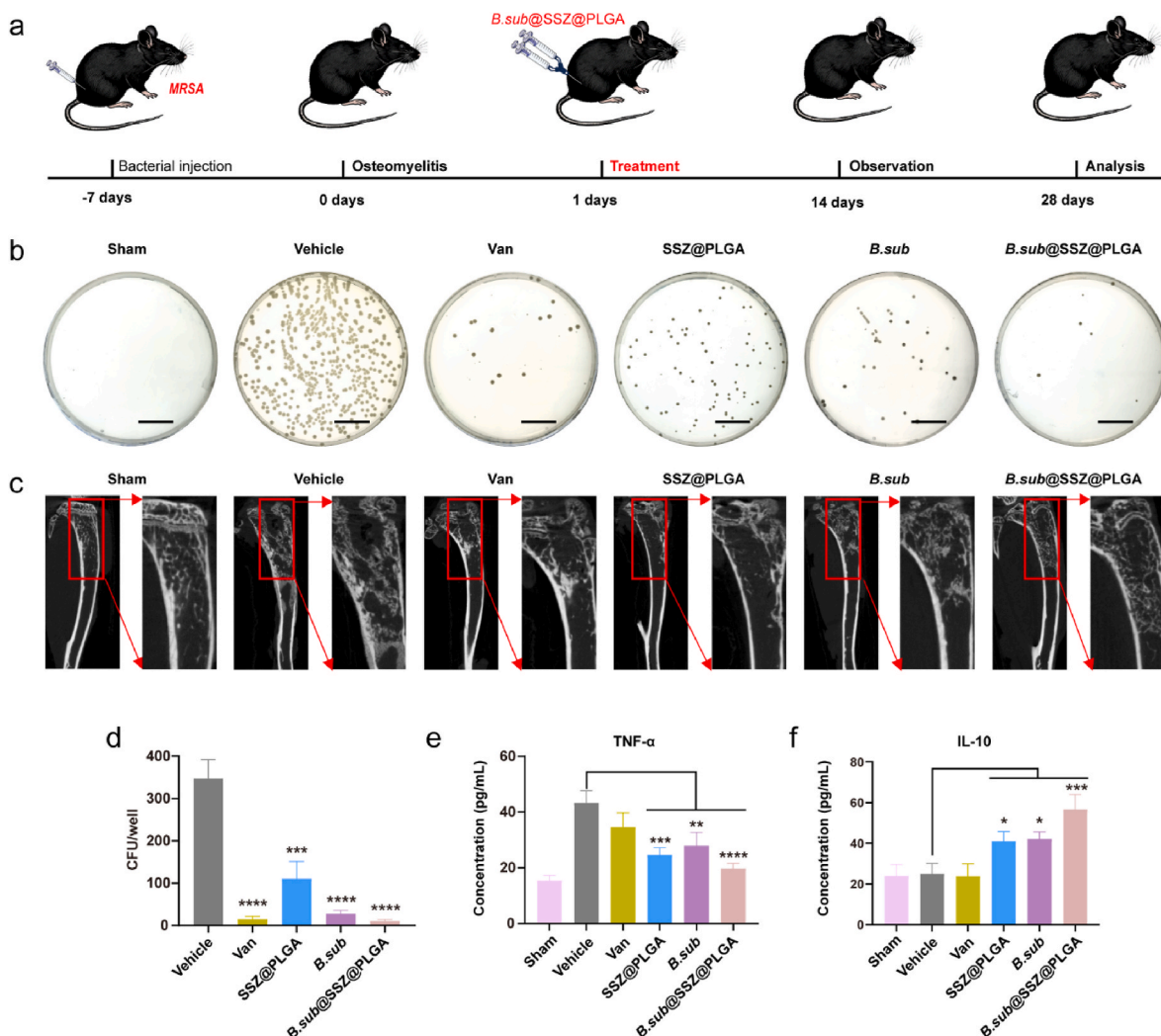


Fig. 6. In vivo osteomyelitis model. (a) Schematic representation of osteomyelitis model and treatment process of *B. sub*@SSZ@PLGA hydrogel. (b) Representative images of bacterial colonies of bone marrow plate after 28 days of treatment. The scale bar is 2 cm. (c) Micro-CT images of the tibias under different treatment. (d) Analysis of bacterial colonies of bone marrow plate after 28 days of treatment. (e) The expression of TNF- α was detected by ELISA kit in blood samples. (f) The expression of IL-10 was detected by ELISA kit in blood samples. Data are presented as mean \pm SD ($n = 6$) (* $P < 0.05$, ** $P < 0.01$, *** $P < 0.001$, **** $P < 0.0001$).

counting (Fig. S11). We observed significant inflammatory destruction of bone tissue in the medullary cavity of mice implanted with MRSA, with abscess formation in the tibia. Upon confirming the successful model of chronic osteomyelitis, the implant was removed, and the medullary cavity was flushed with PBS. Live probiotic hydrogel was then introduced according to the intervention groups. After 28 days of treatment, medullary fluid was collected, and colony counting was performed using the gradient dilution plating method to evaluate antibacterial efficacy. As shown in Fig. 6b and d, compared to the positive control group (Vehicle), the MRSA colony count was slightly reduced in the SSZ@PLGA group, while the Vancomycin (Van), *B. sub* and *B. sub*@SSZ@PLGA groups showed a significant reduction, with inhibition efficiencies of 95.6 % (Van), 92 % (*B. sub*), and 97.1 % (*B. sub*@SSZ@PLGA), respectively. A single injection of engineered probiotic hydrogel demonstrated antibacterial efficacy that was comparable to or even stronger than multiple injection of vancomycin, indicating that live *B. sub* provided more sustained antibacterial effects in vivo. To further assess bone regeneration in the medullary cavity, we measured bone mass using Micro-CT to measure. The results showed uneven distribution of bone trabeculae, medullary cavity voids, bone destruction and abnormal bone tissue proliferation in the Vehicle group (Fig. 6c, Fig. S12). In contrast, the *B. sub*@SSZ@PLGA group exhibited evenly distributed bone trabeculae and no significant medullary cavity voids, with a notable increase in normal bone trabecular tissue compared to the SSZ@PLGA and *B. sub* groups. The *B. sub* group showed increased cancellous bone compared to the Vehicle group, but with abnormal bone trabecular structure. This suggested that bioactive substances secreted by *B. sub* could promote bone regeneration, but their effect on the inflammatory bone microenvironment was limited, leading to abnormal bone trabecular structure. However, in the *B. sub*@SSZ@PLGA group, the inclusion of SSZ improved the bone microenvironment by converting pro-inflammatory macrophages to anti-inflammatory macrophages, allowing the bioactive substances secreted by *B. sub* to better promote angiogenesis and osteogenic differentiation.

To further verify the biosafety of the live probiotic hydrogel in vivo, H&E staining of major organs was performed after 28 days of treatment, revealing no significant lesions (Fig. S13). Blood samples from each group were analyzed using TNF- α and IL-10 ELISA kits, showing a downregulation of the pro-inflammatory factor TNF- α and an upregulation of the anti-inflammatory factor IL-10 in the *B. sub*@SSZ@PLGA group, consistent with our findings in vitro (Fig. 6e and f). Blood biochemical tests also indicated no significant impact of the live probiotic hydrogel on hepatorenal function (Fig. S14), suggesting that the *B. sub*@SSZ@PLGA hydrogel was biologically safe with negligible side effects in mice. Although the Van group showed significant antibacterial effects, blood biochemical tests revealed borderline kidney function, indicating potential nephrotoxicity, highlighting the need for alternative therapies.

To further investigate the impact of the live probiotic hydrogel on promoting bone regeneration in vivo, we performed hematoxylin and eosin stain (H&E) staining and Masson staining to examine the bone formation, and immunofluorescence staining to detect the expression of inflammation-related proteins, osteogenesis-related proteins and angiogenesis-related proteins. As shown in Fig. 7a and Fig. S15, the results showed that *B. sub* and *B. sub*@SSZ@PLGA group tibial medullary cavity could observe more tissue of bone trabecular compared another group. These findings suggested that the live probiotic hydrogel provides a conducive environment for new bone formation. As shown in Fig. 7b and e, the pro-inflammatory protein TNF- α had the highest expression in Vehicle group, while it was significantly downregulated in the SSZ@PLGA group and *B. sub*@SSZ@PLGA group. Conversely, the anti-inflammatory protein CD206 was significantly upregulated in the SSZ@PLGA group and *B. sub*@SSZ@PLGA group, with the highest levels in the *B. sub*@SSZ@PLGA group. As is well known, immune regulation of the bone microenvironment also plays an important role in bone

repair [49,50]. This shift from a pro-inflammatory to an anti-inflammatory environment aligns with the in vitro results, further confirming that the *B. sub*@SSZ@PLGA hydrogel promotes a favorable microenvironment for bone regeneration by reducing inflammation. Additionally, the expression of osteogenesis-related proteins (RUNX2 and COL-1) and angiogenesis-related proteins (CD31 and VEGF) was assessed through immunofluorescence staining and quantification (Fig. 7c, d, f, g). The results revealed significant upregulation of these markers in the *B. sub*@SSZ@PLGA group compared to other groups, indicating enhanced osteogenic differentiation and microvascular formation. To further validate these effects, we conducted qPCR analysis to assess the expression of key genes associated with osteogenesis, angiogenesis, and inflammation in vivo. The results confirmed that RUNX2, COL-1, CD31, VEGF, and CD206 were significantly upregulated under treated with *B. sub*@SSZ@PLGA hydrogel, while TNF- α was downregulated (Fig. 7h, i, j), consistent with the in vitro findings. This alignment between in vitro and in vivo results highlights the ability of the *B. sub*@SSZ@PLGA hydrogel to modulate the inflammatory microenvironment, promote osteogenic differentiation, enhance angiogenesis, and ultimately facilitate bone regeneration.

In summary, the *B. sub*@SSZ@PLGA hydrogel beads exhibited a synergistic triple effect, making them a promising therapeutic strategy for chronic osteomyelitis and bone regeneration. First, the hydrogel released antimicrobial peptides (surfactin, fengycin, and iturin) from *B. sub*, effectively killing MRSA and reducing bacterial colonization. Second, bioactive substances secreted by the probiotics promoted angiogenesis and osteogenesis, as evidenced by increased expression of markers such as CD31, VEGF, RUNX2, and COL-1. Lastly, the incorporation of SSZ further modulated the bone immune microenvironment, transforming it from a pro-inflammatory state to an anti-inflammatory state by reducing TNF- α levels and enhancing CD206 expression. This comprehensive approach not only treated infection but also supported vascularization, bone remodeling, and regeneration, while ensuring biosafety with minimal systemic toxicity.

3. Conclusions

In summary, we designed *B. sub*@SSZ@PLGA biohybrids, encapsulated in alginate hydrogel, which demonstrated excellent antibacterial properties against MRSA both in vitro and in vivo through the secretion of antimicrobial peptides (surfactin, fengycin, and iturin). Additionally, SSZ can transform the pro-inflammatory environment of chronic osteomyelitis into an anti-inflammatory one, thereby improving the bone microenvironment and reducing the immunogenicity of *B. sub*. The bioactive substances secreted by *B. sub* more effectively promote angiogenesis and osteogenic differentiation. Compared to extracting bioactive substances from *B. sub*, using live probiotics offers the advantage of continuously releasing antibacterial agents, which prolongs the effect of a single treatment, enables localized delivery without the need for high doses, and reduces the risk of drug resistance development. Currently, live *B. sub* has clinical applications in oral formulations (Combined *Bacillus subtilis* and *Enterococcus Faecium* Granules with Multivitamins, Live) and topical formulations (*Bacillus subtilis* Preparation for Spraying). However, localized internal applications lack specific formulations. Our study on *B. sub*@SSZ@PLGA hydrogel offers promising prospects for the treatment of localized chronic osteomyelitis.

CRedit authorship contribution statement

Fang-Sheng Fu: Writing – original draft, Investigation, Conceptualization. **Huan-Huan Chen:** Writing – original draft, Investigation, Conceptualization. **Yu Chen:** Investigation. **Ying Yuan:** Investigation. **Yong Zhao:** Investigation. **Aixi Yu:** Writing – review & editing, Supervision, Conceptualization. **Xian-Zheng Zhang:** Writing – review & editing, Supervision, Resources, Project administration, Funding acquisition, Conceptualization.

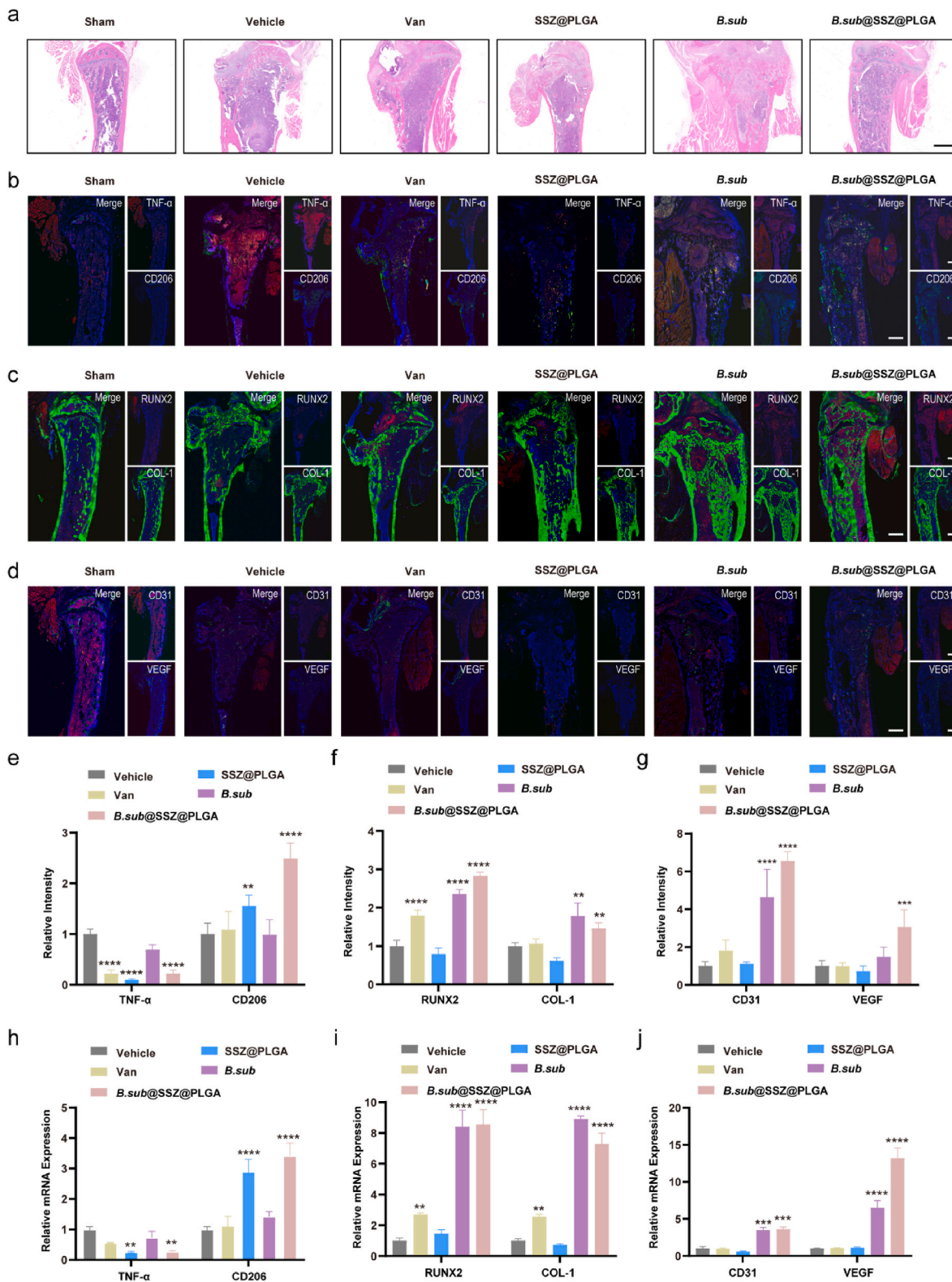


Fig. 7. Anti-inflammatory effects and pro-osteogenesis of *B. sub*@SSZ@PLGA hydrogels in vivo. (a) H&E staining of inflammatory cell infiltration in tibia under different treatments. The scale bar is 1 mm. (b) Immunofluorescence images of TNF- α (red) and CD206 (green) at tibia section in different groups at day 28. The scale bar is 1 mm. (c) Immunofluorescence images of RUNX2 (red) and COL-1 (green) at tibia section under different treatment at day 28. The scale bar is 1 mm. (d) Immunofluorescence images of CD31 (red) and VEGF (green) at tibia section in different groups at day 28. The scale bar is 1 mm. (e) Quantitative analysis of TNF- α and CD206 with ImageJ software. (f) Quantitative analysis of RUNX2 and COL-1 with ImageJ software. (g) Quantitative analysis of CD31 and VEGF with ImageJ software. (h) Inflammation-related genes (TNF- α and CD206) expression after different treatment in vivo. (i) Osteogenesis-related genes (RUNX2 and COL-1) expression after different treatment in vivo. (j) Angiogenesis-related genes (CD31 and VEGF) expression after different treatment in vivo. Data are presented as mean \pm SD (n = 6) (**P < 0.01, ***P < 0.001, ****P < 0.0001).

Experimental section

All details of materials, preparations, characterizations, study methods, and extra data were shown in supporting information.

Ethics approval and consent to participate

All animal experimental protocols were approved by the Institutional Animal Care and Use Committee (IACUC) of the Animal Experiment Center of Wuhan University (Wuhan, P. R. China) (Approval number: ZN2023065).

Declaration of competing interest

The authors declare that they have no known competing financial interests or personal relationships that could have appeared to influence the work reported in this paper.

Acknowledgements

This work was financially supported by the National Natural Science Foundation of China (52333004, 22135005), Xiangyang Joint Fund of Innovation and New Development, Natural Science Foundation of Hubei Province (2022CFD114), the National Key Research and Development Program of China (2019YFA0905603).

Appendix A. Supplementary data

Supplementary data to this article can be found online at <https://doi.org/10.1016/j.bioactmat.2025.01.003>.

References

- C.R. Arciola, D. Campoccia, L. Montanaro, Implant infections: adhesion, biofilm formation and immune evasion, *Nat. Rev. Microbiol.* 16 (7) (2018) 397–409, <https://doi.org/10.1038/s41579-018-0019-y>.
- D.P. Lew, F.A. Waldvogel, Osteomyelitis, *Lancet* (London, England) 364 (9431) (2004) 369–379, [https://doi.org/10.1016/s0140-6736\(04\)16727-5](https://doi.org/10.1016/s0140-6736(04)16727-5).
- Y. Qiao, X. Liu, B. Li, Y. Han, Y. Zheng, K.W.K. Yeung, C. Li, Z. Cui, Y. Liang, Z. Li, S. Zhu, X. Wang, S. Wu, Treatment of MRSA-infected osteomyelitis using bacterial capturing, magnetically targeted composites with microwave-assisted bacterial killing, *Nat. Commun.* 11 (1) (2020) 4446, <https://doi.org/10.1038/s41467-020-18268-0>.
- H. Lin, C. Yang, Y. Luo, M. Ge, H. Shen, X. Zhang, J. Shi, Biomimetic nanomedicine-triggered in situ vaccination for innate and adaptive immunity activations for bacterial osteomyelitis treatment, *ACS Nano* 16 (4) (2022) 5943–5960, <https://doi.org/10.1021/acsnano.1c11132>.
- N. Kavanagh, J.R. Emily, A. Widaa, G. Sexton, J. Fennell, S. O'Rourke, C.C. Kevin, J.K. Cathal, J.O. Fergal, W.K. Steven, Staphylococcal osteomyelitis: disease progression, treatment challenges, and future directions, *Clin. Microbiol. Rev.* 31 (2) (2018), <https://doi.org/10.1128/cmr.00084-17>, 10.1128/cmr.00084-17.
- R.K. Wassif, M. Elkayal, R.N. Shamma, S.A. Elkheshen, Recent advances in the local antibiotics delivery systems for management of osteomyelitis, *Drug Deliv.* 28 (1) (2021) 2392–2414, <https://doi.org/10.1080/10717544.2021.1998246>.
- C. Zhong, Y.M. Wu, H.D. Lin, R.H. Liu, Advances in the antimicrobial treatment of osteomyelitis, *Composites, Part B* 249 (2023) 110428, <https://doi.org/10.1016/j.compositesb.2022.110428>.
- Global burden of bacterial antimicrobial resistance in 2019: a systematic analysis, *Lancet* (London, England) 399 (10325) (2022) 629–655, [https://doi.org/10.1016/s0140-6736\(21\)02724-0](https://doi.org/10.1016/s0140-6736(21)02724-0).
- C.Y. Wang, Y.S. Xia, R.M. Wang, J.R. Li, C. L Chan, R.Y. T. Kao, P.H. Toy, P.L. Ho, H. Y. Li, H.Z. Sun, Metallo-sideromycin as a dual functional complex for combating antimicrobial resistance, *Nat. Commun.* 14 (1) (2023) 5311, <https://doi.org/10.1038/s41467-023-40828-3>.
- J. Dong, W. Wang, W. Zhou, S. Zhang, M. Li, N. Li, G. Pan, X. Zhang, J. Bai, C. Zhu, Immunomodulatory biomaterials for implant-associated infections: from conventional to advanced therapeutic strategies, *Biomater. Res.* 26 (1) (2022) 72, <https://doi.org/10.1186/s40824-022-00326-x>.
- D.J. Davidson, D. Spratt, A.D. Liddle, Implant materials and prosthetic joint infection: the battle with the biofilm, *EFORT open reviews* 4 (11) (2019) 633–639, <https://doi.org/10.1302/2058-5241.4.180095>.
- W. Zimmerli, A. Trampuz, P.E. Ochsner, Prosthetic-joint infections, *N. Engl. J. Med.* 351 (16) (2004) 1645–1654, <https://doi.org/10.1056/NEJMr040181>.
- D.R. Osmon, E.F. Berbari, A.R. Berendt, D. Lew, W. Zimmerli, J.M. Steckelberg, N. Rao, A. Hanssen, W.R. Wilson, Diagnosis and management of prosthetic joint infection: clinical practice guidelines by the Infectious Diseases Society of America, *Clin. Infect. Dis.* 56 (1) (2013) e1–e25, <https://doi.org/10.1093/cid/cis803>.
- S. Chowdhury, S. Castro, C. Coker, T.E. Hinchliffe, N. Arpaia, T. Danino, Programmable bacteria induce durable tumor regression and systemic antitumor immunity, *Nat. Med.* 25 (7) (2019) 1057–1063, <https://doi.org/10.1038/s41591-019-0498-z>.
- D.W. Zheng, Y. Chen, Z.H. Li, L. Xu, C.X. Li, B. Li, J.X. Fan, S.X. Cheng, X.Z. Zhang, Optically-controlled bacterial metabolite for cancer therapy, *Nat. Commun.* 9 (1) (2018) 1680, <https://doi.org/10.1038/s41467-018-03233-9>.
- J.H. Nguyen, V.H. Nguyen, S.N. Jiang, S.H. Park, W. Tan, S.H. Hong, M.G. Shin, I. J. Chung, Y. Hong, H.S. Bom, H.E. Choy, S.E. Lee, J.H. Rhee, J.J. Min, Two-step enhanced cancer immunotherapy with engineered *Salmonella typhimurium* secreting heterologous flagellin, *Sci. Transl. Med.* 9 (376) (2017), <https://doi.org/10.1126/scitranslmed.aak9537>.
- P.W. O'Toole, J.R. Marchesi, C. Hill, Next-generation probiotics: the spectrum from probiotics to live biotherapeutics, *Nat. Microbiol.* 2 (5) (2017) 17057, <https://doi.org/10.1038/nmicrobiol.2017.57>.
- L. Tan, J. Fu, F. Feng, X. Liu, Z. Cui, B. Li, Y. Han, Y. Zheng, K.W.K. Yeung, Z. Li, S. Zhu, Y. Liang, X. Feng, X. Wang, S. Wu, Engineered probiotics biofilm enhances osseointegration via immunoregulation and anti-infection, *Sci. Adv.* 6 (46) (2020), <https://doi.org/10.1126/sciadv.aba5723>.
- E. Noemí, Y. Birsén, S. Heena, K. Manoj, P. Mirian, O. Fatih, L.J. Manuel, A novel approach to *Lactiplantibacillus plantarum*: from probiotic properties to the omics insights, *Microbiol. Res.* 268 (2023) 127289, <https://doi.org/10.1016/j.micres.2022.127289>.
- W.F. van Zyl, S.M. Deane, L.M.T. Dicks, Molecular insights into probiotic mechanisms of action employed against intestinal pathogenic bacteria, *Gut Microb.* 12 (1) (2020) 1831339, <https://doi.org/10.1080/19490976.2020.1831339>.
- F.F. Cao, L.L. Jin, Y. Gao, Y. Ding, H.Y. Wen, Z.F. Qian, C.Y. Zhang, L.J. Hong, H. Yang, J.J. Zhang, Z.R. Tong, W.L. Wang, X.Y. Chen, Z.W. Mao, Artificial-enzymes-armed *Bifidobacterium longum* probiotics for alleviating intestinal inflammation and microbiota dysbiosis, *Nat. Nanotechnol.* 18 (6) (2023) 617–627, <https://doi.org/10.1038/s41565-023-01346-x>.
- Z.Z. Ming, L. Han, M.Y. Bao, H.H. Zhu, S.J. Jiang, S.B. Xue, W.W. Liu, Living bacterial hydrogels for accelerated infected wound healing, *Adv. Sci.* 8 (24) (2021) 2102545, <https://doi.org/10.1002/advs.202102545>.
- R. Mazzolini, I. Rodríguez-Arce, L. Fernández-Barat, C. Piñero-Lambea, V. Garrido, A. Rebollada-Merino, A. Motos, A. Torres, M.J. Grilló, L. Serrano, M. Lluch-Senar, Engineered live bacteria suppress *Pseudomonas aeruginosa* infection in mouse lung and dissolve endotracheal-tube biofilms, *Nat. Biotechnol.* 41 (8) (2023) 1089–1098, <https://doi.org/10.1038/s41587-022-01584-9>.
- Y. Jin, Y. Lu, X. Jiang, M. Wang, Y. Yuan, Y. Zeng, L. Guo, W. Li, Accelerated infected wound healing by probiotic-based living microneedles with long-acting antibacterial effect, *Bioact. Mater.* 38 (2024) 292–304, <https://doi.org/10.1016/j.bioactmat.2024.05.008>.
- Z. Xu, X. Yu, F. Gao, M. Zang, L. Huang, W. Liu, J. Xu, S. Yu, T. Wang, H. Sun, J. Liu, Fighting bacteria with bacteria: a biocompatible living hydrogel patch for combating bacterial infections and promoting wound healing, *Acta Biomater.* 181 (2024) 176–187, <https://doi.org/10.1016/j.actbio.2024.04.047>.
- M. Lufton, Or Bustan, B.H. Eylon, E. Shtifman-Segal, T. Croitoru-Sadger, A. Shagan, A. Shabtay-Orbach, E. Corem-Salkmon, J. Berman, A. Nyska, B. Mizrahi, Living bacteria in thermoresponsive gel for treating fungal infections, *Adv. Funct. Mater.* 28 (40) (2018) 1801581, <https://doi.org/10.1002/adfm.201801581>.
- P. Piewngam, Y. Zheng, T.H. Nguyen, Seth W. Dickey, H.S. Joe, A.E. Villaruz, K. A. Glose, E.L. Fisher, R.L. Hunt, B. Li, J. Chiou, S. Pharkjaksu, S. Khongthong, G.Y. C. Cheung, P. Kiratisin, M. Otto, Pathogen elimination by probiotic *Bacillus* via signalling interference, *Nature* 562 (7728) (2018) 532–537, <https://doi.org/10.1038/s41586-018-0616-y>.
- P. Piewngam, S. Khongthong, N. Roekngam, Y. Theapparatt, S. Sunpaweravong, D. Faroongsarng, M. Otto, Probiotic for pathogen-specific *Staphylococcus aureus* decolonisation in Thailand: a phase 2, double-blind, randomised, placebo-controlled trial, *Lancet Microbe* 4 (2) (2023) e75–e83, [https://doi.org/10.1016/s2666-5247\(22\)00322-6](https://doi.org/10.1016/s2666-5247(22)00322-6).
- A. Richter, F. Blei, G. Hu, J.W. Schwitalla, C.N. Lozano-Andrade, J. Xie, S. A. Jarmusch, M. Wibowo, B. Kjeldgaard, S. Surabhi, X. Xu, T. Jautzus, C.B. W. Phippen, O. Tyc, M. Arentshorst, Y. Wang, P. Garbeva, T.O. Larsen, A.F.J. Ram, C.A.M. van den Hondel, G. Maróti, T. Kovács Á, Enhanced surface colonisation and competition during bacterial adaptation to a fungus, *Nat. Commun.* 15 (1) (2024) 4486, <https://doi.org/10.1038/s41467-024-48812-1>.
- J. Liu, W. Li, X. Zhu, H. Zhao, Y. Lu, C. Zhang, Z. Lu, Surfactin effectively inhibits *Staphylococcus aureus* adhesion and biofilm formation on surfaces, *Appl. Microbiol. Biotechnol.* 103 (11) (2019) 4565–4574, <https://doi.org/10.1007/s00253-019-09808-w>.
- M. Lefevre, S.M. Racedo, G. Ripert, B. Housez, M. Cazaubiel, C. Maudet, P. Jüsten, P. Marteau, M.C. Urdaci, Probiotic strain *Bacillus subtilis* CU1 stimulates immune system of elderly during common infectious disease period: a randomized, double-blind placebo-controlled study, *Immun. Age* (Chester) 12 (1) (2015) 24, <https://doi.org/10.1186/s12979-015-0051-y>.
- M.A. Peppercorn, Sulfasalazine. Pharmacology, clinical use, toxicity, and related new drug development, *Ann. Intern. Med.* 101 (3) (1984) 377–386, <https://doi.org/10.7326/0003-4819-101-3-377>.
- E.C. Keystone, M.M. Wang, M. Layton, S. Hollis, I.B. McInnes, Clinical evaluation of the efficacy of the P2X7 purinergic receptor antagonist AZD9056 on the signs and symptoms of rheumatoid arthritis in patients with active disease despite treatment with methotrexate or sulphasalazine, *Ann. Rheum. Dis.* 71 (10) (2012) 1630–1635, <https://doi.org/10.1136/annrheumdis-2011-143578>.

- [34] B. Yang, W. Shu, J. Hu, Z. Wang, J. Wu, J. Su, J. Tan, B. Yu, X. Zhang, Aberrant expression of SLC7A11 impairs the antimicrobial activities of macrophages in staphylococcus aureus osteomyelitis in mice, *Int. Biol. Sci.* 20 (7) (2024) 2555–2575, <https://doi.org/10.7150/ijbs.93592>.
- [35] V. Nele, J.P. Wojciechowski, J.P.K. Armstrong, M.M. Stevens, Tailoring gelation mechanisms for advanced hydrogel applications, *Adv. Funct. Mater.* 30 (42) (2020) 2002759, <https://doi.org/10.1002/adfm.202002759>.
- [36] L.C. Xia, H. Huang, Z. Fan, D.W. H, D.M. Zhang, A.S. Khan, M. Usman, L.J. Pan, Hierarchical macro-/meso-/microporous oxygen-doped carbon derived from sodium alginate: a cost-effective biomass material for binder-free supercapacitors, *Mater. Des.* 182 (2019) 108048, <https://doi.org/10.1016/j.matdes.2019.108048>.
- [37] A.M. Earl, R. Losick, R. Kolter, Ecology and genomics of *Bacillus subtilis*, *Trends Microbiol.* 16 (6) (2008) 269–275, <https://doi.org/10.1016/j.tim.2008.03.004>.
- [38] M. Fujiya, M.W. Musch, Y. Nakagawa, S. Hu, J. Alverdy, Y. Kohgo, O. Schneewind, B. Jabri, E.B. Chang, The *Bacillus subtilis* quorum-sensing molecule CSF contributes to intestinal homeostasis via OCTN2, a host cell membrane transporter, *Cell Host Microbe* 1 (4) (2007) 299–308, <https://doi.org/10.1016/j.chom.2007.05.004>.
- [39] A. Sica, M. Erreni, P. Allavena, C. Porta, Macrophage polarization in pathology, *Cell. Mol. Life Sci.* 72 (21) (2015) 4111–4126, <https://doi.org/10.1007/s00018-015-1995-y>.
- [40] H. Xiao, Y. Guo, B. Li, X. Li, Y. Wang, S. Han, D. Cheng, X. Shuai, M2-Like tumor-associated macrophage-targeted codelivery of STAT6 inhibitor and IKK β siRNA induces M2-to-M1 repolarization for cancer immunotherapy with low immune side effects, *ACS Cent. Sci.* 6 (7) (2020) 1208–1222, <https://doi.org/10.1021/acscentsci.9b01235>.
- [41] Z. Chen, A. Bachhuka, F. Wei, X. Wang, G. Liu, K. Vasilev, Y. Xiao, Nanotopography-based strategy for the precise manipulation of osteoimmunomodulation in bone regeneration, *Nanoscale* 9 (46) (2017) 18129–18152, <https://doi.org/10.1039/c7nr05913b>.
- [42] Y. Wang, H. Liu, J. Zhao, Macrophage polarization induced by probiotic bacteria: a concise review, *Probiotics Antimicrob* 12 (3) (2020) 798–808, <https://doi.org/10.1007/s12602-019-09612-y>.
- [43] N. Liu, J.L. Zhang, M.Z. Yin, H. Liu, X. Zhang, J.D. Li, B. Yan, Y.Y. Guo, J.D. Zhou, J. Tao, S. Hu, X. Chen, C. Peng, Inhibition of xCT suppresses the efficacy of anti-PD-1/L1 melanoma treatment through exosomal PD-L1-induced macrophage M2 polarization, *Mol. Ther.* 29 (7) (2021) 2321–2334, <https://doi.org/10.1016/j.ymthe.2021.03.013>.
- [44] T.R. Kuo, C.H. Chen, Bone biomarker for the clinical assessment of osteoporosis: recent developments and future perspectives, *Biomark. Res.* 5 (2017) 18, <https://doi.org/10.1186/s40364-017-0097-4>.
- [45] J. Filipowska, K.A. Tomaszewski, Ł. Niedźwiedzki, J.A. Walocha, T. Niedźwiedzki, The role of vasculature in bone development, regeneration and proper systemic functioning, *Angiogenesis* 20 (3) (2017) 291–302, <https://doi.org/10.1007/s10456-017-9541-1>.
- [46] X.D. Zhang, Z.X. Wang, Q. Liu, X.L. Hui, J.W. Mei, D.D. Xu, J. Zhou, X.Z. Zhang, Q. M. Li, H. Chen, Z. Su, W.B. Zhu, C. Zhu, Targeted modulation and enhancement of macrophages via sonodynamic therapy-driven cupferroptosis-like stress for implant-associated biofilm infections, *Nano Today* 54 (2024) 102092, <https://doi.org/10.1016/j.nantod.2023.102092>.
- [47] B.H. Kapadia, R.A. Berg, J.A. Daley, J. Fritz, A. Bhavne, M.A. Mont, Periprosthetic joint infection, *Lancet* 387 (10016) (2016) 386–394, [https://doi.org/10.1016/s0140-6736\(14\)61798-0](https://doi.org/10.1016/s0140-6736(14)61798-0).
- [48] B.R. Boles, M. Thoendel, A.J. Roth, A.R. Horswill, Identification of genes involved in polysaccharide-independent *Staphylococcus aureus* biofilm formation, *PLoS One* 5 (4) (2010) e10146, <https://doi.org/10.1371/journal.pone.0010146>.
- [49] S.T. Zhang, H.T. Yang, M.Q. Wang, D. Mantovani, K. Yang, F. Witte, L.L. Tan, B. Yue, X.H. Qu, Immunomodulatory biomaterials against bacterial infections: progress, challenges, and future perspectives, *Innovation* 4 (6) (2023) 100503, <https://doi.org/10.1016/j.xinn.2023.100503>.
- [50] L.P. Tong, W.A.J. van, H.Y. Wang, D. Chen, Advancing bone biology: the mutual promotion of biology and pioneering technologies, *The Innovation Life* 2 (3) (2024) 100078, <https://doi.org/10.59717/j.xinn-life.2024.100078>.